ACS APPLIED MATERIALS & INTERFACES

Research Article

www.acsami.org

# Highly Transparent and Toughened Poly(methyl methacrylate) Nanocomposite Films Containing Networks of Cellulose Nanofibrils

Hong Dong,*[†,‡,§] Yelena R. Sliozberg,[†,‡] James F. Snyder,[†] Joshua Steele,[†] Tanya L. Chantawansri,[†] Joshua A. Orlicki,[†] Scott D. Walck,[†,‡] Richard S. Reiner,[∥] and Alan W. Rudie[∥]

[†]Macromolecular Science & Technology Branch, U.S. Army Research Laboratory, Aberdeen Proving Ground, Maryland 21005, United States

[‡]TKC Global Solutions, LLC, Aberdeen, Maryland 21005, United States

[∥]Forest Products Laboratory, USDA Forest Service, Madison, Wisconsin 53726, United States

Supporting Information

**ABSTRACT:** Cellulose nanofibrils (CNFs) are a class of cellulosic nanomaterials with high aspect ratios that can be extracted from various natural sources. Their highly crystalline structures provide the nanofibrils with excellent mechanical and thermal properties. The main challenges of CNFs in nanocomposite applications are associated with their high hydrophilicity, which makes CNFs incompatible with hydrophobic polymers. In this study, highly transparent and toughened poly(methyl methacrylate) (PMMA) nanocomposite films were prepared using various percentages of CNFs covered with surface carboxylic acid groups (CNF-COOH). The surface groups make the CNFs interfacial interaction with PMMA favorable, which facilitate the homogeneous dispersion of the hydrophilic nanofibrils in the hydrophobic polymer and the formation of a percolated network of nanofibrils. The controlled dispersion results in high transparency of the nanocomposites. Mechanical analysis of the resulting films demonstrated that a low percentage loading of CNF-COOH worked as effective reinforcing agents, yielding more ductile and therefore tougher films than the neat PMMA film. Toughening mechanisms were investigated through coarse-grained simulations, where the results demonstrated that a favorable polymer-nanofibril interface together with percolation of the nanofibrils, both facilitated through hydrogen bonding interactions, contributed to the toughness improvement in these nanocomposites.

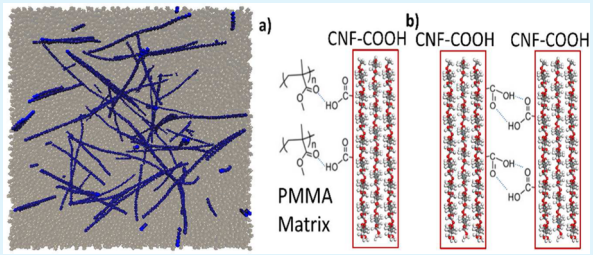


**KEYWORDS:** *cellulose nanofibrils, poly(methyl methacrylate), nanocomposites, interfacial interactions, mechanical properties, coarse-grained simulation*

## INTRODUCTION

Nanocellulose is described as "the sustainable materials of choice for the 21st century".[1] Cellulose nanofibrils (CNFs) are a class of nanocellulose materials with unique properties and many potential applications. Their internal hydrogen bonding between cellulose chains and interspersed crystalline regions provide the nanofibrils with excellent mechanical and thermal properties, including high modulus, high strength, and a low coefficient of thermal expansion.[1−3] These nanofibrils have been proposed for many potential applications, such as reinforcement fillers for polymer composites, rheology control for liquids, optically transparent composites for flexible electronics and in improved barrier membranes.[1,4] As a general class of nanoscale particles, cellulose nanofibrils are produced by a wide variety of methods that result in a variety of particle sizes and forms. The dimensions of CNFs can vary substantially, depending on the degrees of fibrillation and pretreatment involved, usually between 4−20 nm in width, and 500−2000 nm in length.[2] The nanofibrils used in this study were prepared using TEMPO (2,2,6,6-tetramethylpiperidine-1-oxyl radical)-mediated oxidation and disintegration,[3] where the process results in C6 carboxylate groups selectively formed on the nanofibril surface.

CNFs have been used as reinforcement nanofillers for polymer nanocomposites. Compared with cellulose nanocrystals, cellulose nanofibrils have high aspect ratios that enable formation of a percolated network at a low concentration in polymer matrices. The fibril−fibril interactions caused by the percolation contribute to further improvement in the mechanical properties of the composite.[5] Moreover, the fibril diameter, being far below the wavelength of visible light, enables the reinforcement of transparent polymers without compromising their optical properties. Because of the hydrophilic nature of cellulose, cellulose nanofibrils are commonly used to reinforce hydrophilic polymers, such as poly(ethylene oxide) (PEO)[5] and poly(vinyl alcohol) (PVA).[6] Significant improvements in strength, modulus and fracture toughness have been achieved for solution-cast PEO composite films.

Received: September 8, 2015
Accepted: October 29, 2015
Published: October 29, 2015

ACS Publications © 2015 American Chemical Society



DOI: 10.1021/acsami.5b08317
ACS Appl. Mater. Interfaces 2015, 7, 25464−25472

These increases were attributed to CNFs high mechanical properties, good dispersion and strong interfacial hydrogen bonding between cellulose and the matrix.[5]

Even so, the main challenges of utilizing CNFs in composite applications are associated with the high hydrophilicity, which makes them incompatible with hydrophobic polymers. The hydrophilic nature, along with their inherent tendency to form aggregates held together by hydrogen bonding, impedes dispersing CNFs in hydrophobic polymers and therefore leads to lower mechanical properties of the composites than predicted. To address this deficiency, researchers investigated surface modifications based on polymer grafting, coupling agents, acetylation, and cationic modification to improve compatibility and dispersion in polymer matrices.[4,7] As an example, cellulose nanocrystals and microfibrils were chemically modified with N-octadecyl isocyanate, where the chemical grafting was found to improve compatibility with polycaprolactone and dispersity.[8] Polystyrene containing various ratios of dispersed TEMPO-oxidized cellulose nanofibrils exhibited increases in tensile strength and elastic modulus. The reinforcement effects were observed even at low addition levels in relation to the neat film.[9] In many studies, improvements to the modulus of hydrophobic polymers through reinforcement with cellulose nanofibrils was coupled with a reduction in toughness due to reduced elongation at break. This increased brittleness may be associated with nanofibril aggregation in hydrophobic polymers or weak hydrophilic nanofiller−hydrophobic matrix interfaces. Because effective utilization of nanofillers in composite applications depends strongly on their ability to be dispersed homogeneously within a polymer matrix as well as interfacial interactions,[10,11] an optimized interfacial interaction between CNFs and hydrophobic polymer matrix and good dispersion of CNFs should lead to efficient load transfer to the hard component of the composite and/or allow for significant energy dissipation without macroscopic failure, resulting in enhanced mechanical properties of the materials.

Poly(methyl methacrylate) (PMMA) is a commonly employed glassy thermoplastic polymer. Because of excellent transparency in the visible spectrum, PMMA is widely used in optical applications, especially as a matrix for nonlinear optical materials. However, applicability is limited by relatively high brittleness. Incorporation of reinforcing fillers, such as CNFs, into a PMMA matrix could result in an enhanced material. Previously reported work includes composites prepared by solution blending of PMMA and PMMA-grafted CNFs followed by injection and compression molding. The tensile testing showed no improvement of the mechanical properties and the transparency of the composites was notably decreased, because of the visible heterogeneity of the composites caused by insufficient mixing of the components.[12]

This study focuses on incorporating TEMPO-oxidized CNFs into PMMA as an approach to improve toughness while maintaining optical transparency. In this work, low percentages of modified CNFs, where carboxylate groups on the nanofibrils were protonated to carboxylic acid groups, were mixed in a PMMA matrix. The effect of incorporating CNFs into PMMA was studied by microscopy, thermal analysis, and mechanical testing. This, together with modeling the mechanism for material failure, provides further insight on CNF reinforced hydrophobic polymers. Computational models at the coarse-grained level were used to understand the fundamental mechanism responsible for toughening of these materials. Computed results are shown to have good qualitative agreement with experimental data obtained for the PMMA nanocomposite films containing low percentages of carboxyl CNFs.

## ■ EXPERIMENTAL SECTION

**Materials.** Aqueous dispersion of carboxylated cellulose nanofibrils (balanced with sodium ions, noted as CNF-COONa) nanofibrils were produced from wood pulp using the TEMPO oxidation technique and sodium hypochlorite as the stochiometric oxidant.[13] The water dispersion of CNFs used in this study has a concentration of 1.0 wt % and a surface carboxylate content of 1.3 mmol/g. Poly(methyl methacrylate) (PMMA), N,N-dimethylformamide (DMF), and all other chemicals were of analytical grade and used as received. Deionized water with resistance ∼18.2 MΩ m was used in all experiments.

**Preparation of CNF-COOH/PMMA Film.** The "as-produced" TEMPO-oxidized CNFs carry surface sodium carboxylate groups, which is described as CNF-COONa in this report. CNF-COONa was protonated to CNF-COOH using a method adapted from Isogai's group.[14] Briefly, 1.0 wt % CNF-COONa was diluted to 0.1 wt % in $H_2O$, which was adjusted to pH ∼2 with 1 N HCl. Gel particles of CNF-COOH were obtained by centrifuging to remove water from the mixture. The gel particles were then washed and centrifuged repeatedly with $H_2O$ several times. The CNF-COOH in $H_2O$ particles was completely solvent-exchanged to acetone by repeatedly adding acetone and centrifuging to remove solvent. DMF was then added to the CNF-COOH particles in acetone. The mixture was evaporated using a rotary evaporator under vacuum and at 50 °C to remove acetone. The concentration of suspended CNF-COOH/DMF particles was determined by dry weight. Clear dispersion of CNF-COOH in DMF was obtained by diluting the concentrated CNF-COOH/DMF with DMF and sonicating in a water-bath sonicator (Fisher Scientific, FS30H) for 30 min to 1 h. The dispersion after sonication was examined using a cross polarizer. The presence of flow birefringence and absence of gel particles were used to indicate good dispersion. The dispersion was further examined using transmission electron microscopy as described below.

To prepare the nanocomposite films, 5 g of PMMA dissolved in DMF was mixed with CNF-COOH/DMF dispersion and stirred for at least 1 h. The weight ratio of CNF-COOH in the PMMA/CNF-COOH was varied from 0 to 5 wt %. The solution of CNF-COOH/PMMA in DMF was cast in a glass crystallizing dish. The solution was dried in an oven purged with nitrogen gas at a temperature below 40 °C. The PMMA/CNF-COOH nanocomposite films thus formed were detached from glass dishes and vacuum-dried at 50 °C for several days. The resulting PMMA/CNF-COOH nanocomposite films were ∼0.2 mm in thickness.

**Characterizations.** *Electron Microscopy.* The dispersions of nanofibrils in solvents were characterized using a JEOL 2100F transmission electron microscope (TEM) operated at 200 kV. For the TEM samples of the CNF dispersion in $H_2O$ or the CNF-COOH dispersion in DMF, the TEM grid covered with an ultrathin carbon film was treated with air plasma for 45 s to increase hydrophilicity of the carbon support film and thus prevent aggregation of the nanofibrils dried on the grid. A droplet of the diluted nanofibril dispersion was cast on the grid and remained on the grid for 1 min. Then the extra fluid was removed with the edge of filter paper, and the remaining nanofibrils were stained with 2% aqueous solution of uranyl acetate before being air-dried in order to enhance the TEM image contrast. To examine the dispersion of CNF-COOH in the nanocomposite film, we embedded the film in EPO-FIX embedding epoxy resin (Electron Microscopy Sciences) and cured overnight at room temperature. The embedded film was then cross-sectioned using a Leica microtome. The sliced thin sections with thickness ∼100 nm were collected on the TEM grids and stained with 2% uranyl acetate. The dispersion of nanofibrils in the nanocomposte films was investigated using the JEOL 2100F scope with scanning transition electron microscopy (STEM) mode. Bright-field (BF) STEM images were acquired using a JEOL BF


DOI: 10.1021/acsami.5b08317
ACS Appl. Mater. Interfaces 2015, 7, 25464−25472

detector. High-angle annular dark-field (HAADF) images were acquired with a Gatan 806 HAADF detector. The fracture surfaces of the tensile samples were characterized using a Hitachi S-4700 field-emission scanning electron microscope (FESEM) at an accelerating voltage of 5 kV. The samples were sputter-coated with Au/Pt alloy to reduce charging before FESEM operation.

*Thermal Analysis.* Differential scanning calorimetry (DSC) was performed using a TA DSC Q1000 instrument. The tests were carried out at a ramping rate of 10 °C/min from room temperature to 200 °C under a nitrogen atmosphere.

*UV−Vis Spectroscopy.* UV−vis spectra of the films were collected at a wavelength range of 250 to 900 nm using a Beckman Coulter DU 800 spectrophotometer. The transmission spectra were acquired on the free-standing films using air as blank.

*Dynamic Mechanical Analysis.* Dynamic mechanical analysis (DMA) of the composite films was conducted using a DMA Q800 (TA Instruments) equipped with a film tension clamp. Tests were run from −20 to 120 °C at a rate of 3 °C/min. Oscillation amplitude of 5 μm (within linear range) was applied on all samples. At least three repeats were tested for each sample.

*Tensile Testing.* Uniaxial tensile loading was performed on flat, dogbone test specimens based on the dimensions in ASTM D638. Test specimens were laser-cut into dog-bone geometries from the cast thin films. An Instron model 1122 load frame with a 50 N load cell was used to carry out the tests. The specimens were loaded in tension at a cross-head speed of 12 mm/min. The load and displacement values were recorded and the strain was calculated using digital image correlation.

## ■ COMPUTATIONAL MODEL AND METHODS

Supplementary to experimental efforts, computational modeling provides a powerful means to investigate a broad range of parameters that are challenging to explore experimentally. The complexity and size of these nanocomposite structures restrict the use of all-atom computer simulations. Instead a coarse-grained (CG) representation is utilized to extend the length and time scale accessible to simulation, where atoms are grouped together to form effective interaction sites. The resolution accessible to this simulation method is adequate because the modeling will only be used to elucidate the fundamental mechanism responsible for toughening in PMMA composites containing cellulose nanofibrils. These simulations were performed using the large-scale atomic/molecular massively parallel simulator (LAMMPS).[15,16]

Coarse-grained molecular dynamics simulations of the neat or composite polymer system were performed using the standard generic bead−spring model,[17] which has been shown to be an excellent technique to study the structural, dynamical, and mechanical properties of large variety of polymer systems.[18−21] The simulation box for our pure polymer system is composed of 8000 linear flexible chains, where each chain contains $N_p = 30$ beads. To model the CNF-COOH dispersion in the composite system, we added 50 rigid long rods each composed of $N_r = 50$ beads.

All beads have a mass $m$ and the pair interaction between topologically nonconnected beads is described by the standard truncated Lennard−-Jones (LJ) pair potential

$$U_{LJ}(r) = 4u_0\left[\left(\frac{a}{r}\right)^{12} - \left(\frac{a}{r}\right)^{6} - \left(\frac{a}{r_c}\right)^{12} + \left(\frac{a}{r_c}\right)^{6}\right] \quad (1)$$

where $u_0$ is the depth of the potential well and $a$ represents a size of a bead. We express all quantities in terms of the mass $m$, intermonomer binding energy $u_0$, monomer diameter $a$ and characteristic time $\tau = (ma^2/u_0)^{1/2}$, where we use the standard LJ potential cutoff, $r_c = 2.5a$.

Topologically bound monomers interact according to the standard FENE/Lennard−Jones bonded potential, $U_{FENE/LJ}$

$$U_{FENE/LJ}(r) = U_{FENE}(r) + U_{WCA}(r) \quad (2)$$

and

$$U_{FENE}(r) = -\frac{a_{FENE}}{2}R_0^2\ln\left[1 - \left(\frac{r}{R_0}\right)^2\right] \quad (3)$$

where $U_{FENE}$ is the finite extensible nonlinear elastic potential (FENE). The standard parameter values of the spring constant, $a_{FENE} = 30u_0/a^2$ and the maximum extension, $R_0 = 1.5a$, were employed. The so-called Weeks−Chandler−Andersen excluded volume potential, $U_{WCA}$, is obtained by setting $r_c = 2^{1/6}a$ in eq 1.

The rigidity of the long rods is controlled through a harmonic angular potential

$$U_a(\theta) = k(\theta - \theta_0)^2 \quad (4)$$

where $\theta$ is the angle between triplets of connected beads, $\theta_0 = \pi$ is the equilibrium value of the angle, and $k = 300u_0/rad^2$.

These initial systems were built and first equilibrated by using a fast equilibration protocol.[22] Periodic boundary conditions are applied in all three directions of the initially cubic simulation cells, using a MD time step of $\Delta t = 0.01\ \tau$. Temperature, $T = 1.0u_0/k_BT$, is controlled during the entire simulation by a Langevin thermostat with a damping time of 1.0 $\tau$. Initially, the pair interaction between nonbonded particles is described by the excluded volume potential, $U_{WCA}$. The hydrogen bonding interactions between CNF and polymer matrix are simulated by allowing the polymer chains and the long rods to create FENE bonds, if the distance between attractive sites of polymer chains and rods is less than 1.2$a$. In the polymer chain and rod, we utilized 3 and 25 evenly distributed attractive sites, respectively, where attractive LJ interactions ($r_c = 2.5a$) are used between these sites before reaction. The simulation was allowed to run until all of the polymer chains attractive sites have reacted with those on the rods.

After this step, the LJ potential cutoff, $r_c$ is changed from $2^{1/6}a$ to 2.5$a$ for all monomers. The systems were then quenched from $T = 1.0u_0/k_BT$ to $T = 0.3u_0/k_BT$ at constant volume over a time interval of $1 \times 10^5\ \tau$ to reach a glassy state. The glass transition temperature $T_g$ for the Lennard−Jones polymer[23] is $T_g = 0.5u_0/k_BT$. Finally, the systems were equilibrated at zero hydrostatic pressure, yielding an equilibrium monomer number density $\rho = 0.87a^{-3}$.

After equilibration, simulations of uniaxial-stress tensile deformation in the $z$ direction were performed. The brittleness of PMMA is known to be the result of catastrophic strain localization in the form of crazes, which results in failure prior to the yield point. To simulate craze formation, $L_z$ length is increased at constant engineering strain rate $\dot{\varepsilon} = 1 \times 10^{-4}\ \tau^{-1}$, whereas the other dimensions of the cell are held fixed.[19] For the deformation simulations, the time step is reduced to 0.075$\tau$. Although the employed strain and cooling rates are much higher than typical experimental rates because of limitations in accessible strain rates and equilibration of the initial structure, the stress generally has weak (logarithmic) rate dependence in polymer glasses.[18]

During the deformation process, bonds intrinsic to the polymer or the rods are set to break when the distance between a pair of bonded particles is greater than 1.4$a$, whereas bonds formed between the rods and polymer matrix were allowed to break at shorter distance of 1.3$a$. In our simulations, broken bonds are not allowed to reform. For the composite systems, the deformation simulations were stopped once the rods started to break.

## ■ RESULTS AND DISCUSSION

**Dispersion and Nanocomposite Film Preparation.** Figure 1 shows a TEM image of "as-produced" cellulose nanofibrils that were used in this study. The nanofibrils have an average diameter of ∼4 nm determined by taking measurements from several TEM images. The nanofibrils carry carboxylate groups balanced with sodium ions (CNF-COONa), which provides repulsive charges that aid in the dispersion of nanofibrils in $H_2O$. However, direct dispersion of CNF-COONa by solvent exchange in many common organic solvents is very limited. Upon addition of common organic solvents, gel particles of CNF-COONa form immediately and


DOI: 10.1021/acsami.5b08317
ACS Appl. Mater. Interfaces 2015, 7, 25464−25472

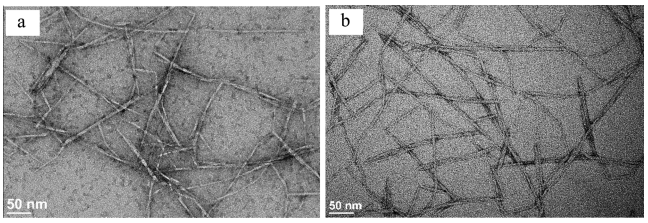


**Figure 1.** Transmission electron microscopic images of (a) "as-produced" CNF-COONa dispersed in $H_2O$ and (b) redispersed CNF-COOH in DMF. The nanofibrils on the TEM grids were stained with 2% uranyl acetate before imaging to enhance image contrast again carbon support films.

cannot be redispersed by sonication. Okita et al.[14] investigated the dispersibility of CNF-COONa and CNF-COOH in various organic solvents. By converting the surface carboxylate groups of CNF-COONa to carboxylic acid groups, the nanofibrils were found to individually disperse in polar aprotic organic solvents such as N,N-dimethylacetamide (DMAc) and DMF at a low concentration.[14] The conversion of the surface carboxylate to carboxylic acid and subsequent dispersion in nonaqueous media can also expand the range of surface chemistry to be performed on the nanofibrils or enable surface interactions with the polymer matrix.

The dispersion of CNF-COOH gel particles in DMF after bath sonication was visually examined using a cross-polarizer, where the absence of visible gel particles and presence of flow birefringence indicate good dispersion of the nanofibrils in the solvent. The sonication process seems to be an efficient way of breaking the weak hydrogen bonds and dispersing nanofibrils in polar organic solvents. However, a recent study showed that intensive high-energy sonication had a major impact on the chain bonding within the cellulose supramolecular structure.[24] In this study, low-energy bath sonication was applied to disperse weakly bonded CNF-COOH gel particles into DMF. To compare the dimension of the redispersed nanofibrils (CNF-COOH) with "as-produced" CNF-COONa nanofibrils, we examined the morphology of dispersed CNF-COOH in DMF under TEM. As shown in Figure 1b, the nanofibrils of CNF-COOH maintain the fibril structure. The average diameter measured from Figure 1b and other TEM images were ∼4 nm with average length ∼440 nm, similar to those of "as-produced" nanofibrils.

PMMA films with different weight ratios of CNF-COOH and neat PMMA film were prepared. Visually, the nanocomposite films have high transparency, comparable to the neat PMMA film, as shown in Figure 2a. The surfaces of the prepared films are very smooth. Further evaluation of the transparency of the PMMA nanocomposite films was performed using UV−vis transmittance. Figure 2b shows that the PMMA/CNF-COOH film containing 0.5 wt % up to 3 wt % of nanofibrils have similar transmittance as that of the neat PMMA film in the range of visible wavelengths. The transmittances at 550 nm were used as relative values to compare the composite films with the neat film. The neat PMMA film displays a transmittance of 92% at 550 nm. PMMA films containing 1 wt % nanofibrils or 3 wt % nanofibrils have same level of light transmittance as that of neat film with both also having a transmittance of 92% at 550 nm. When the content of nanofibrils in PMMA increases to 5 wt %, the light transmittance at 550 nm slightly decreases to 90%. Toward the blue side of the spectrum, such as 450 nm, the transmittance of

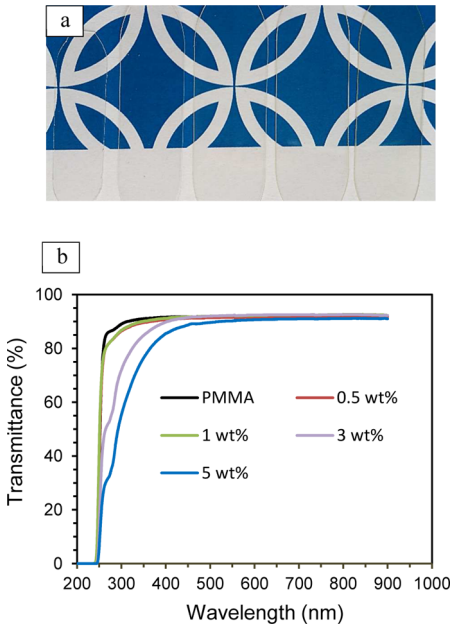


**Figure 2.** (a) Photo (from left to right: PMMA, 0.5 wt %, 1, 3, and 5 wt %) and (b) UV−vis absorption of the neat PMMA film and the PMMA/CNF-COOH nanocomposite films.

5 wt % further decreases compared with other contents. This indicates some aggregation of nanofibrils in PMMA matrix.

The dispersion of 3 wt % CNF-COOH in PMMA film was investigated by the microtome technique and scanning transmission electron microscopic (STEM) examination. Figure 3 shows a bright field image for a cross-sectional

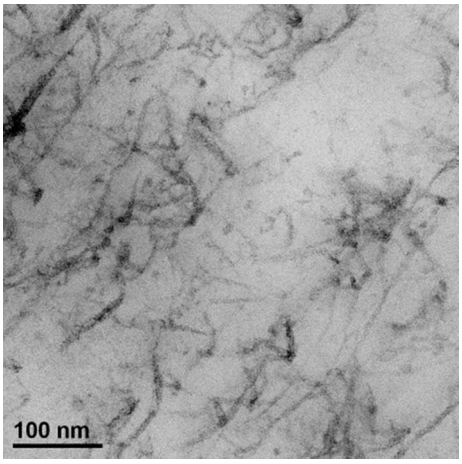


**Figure 3.** Scanning transmission electron microscopic (STEM) bright-field images of cross-sectional PMMA/CNF-COOH (3 wt %) nanocomposite film.

PMMA film containing 3 wt % CNF-COOH. A high-angle annular dark-field (HAADF) image was provided in Figure S1. The thin sections of the nanocomposite film were stained with uranyl acetate before imaging. It is well-established that carboxylate or carboxylic acid groups bind strongly with metal ions,[25] whereas PMMA has only a weak affinity to metal ions.[26] It is evident that the black fibril structure in the bright-field image (Figure 3) and the white fibril structure in the dark-field image (Figure S1) comes from the nanofibrils within the PMMA matrix. At 3 wt % the nanofibrils are well-


DOI: 10.1021/acsami.5b08317
ACS Appl. Mater. Interfaces 2015, 7, 25464−25472

dispersed to form an interconnected long-range network structure in the PMMA matrix with little aggregation. Samples with lower CNF contents should have a similar level of dispersion because of similar level of film transparency at visible range. At 5% CNF content, the CNFs are expected to be well-dispersed, but a small portion of the CNFs are aggregated on the basis of UV−vis results.

**Thermal Property and Interactions.** Dynamic thermal analysis (DSC) was performed on the nanocomposites and the neat polymer to evaluate the influence of CNF−COOH on the thermal transition of PMMA. Addition of as little as 0.5 wt % of CNF-COOH significantly increases the glass transition temperature ($T_g$) compared to the neat PMMA (Table 1 and Figure S2). The $T_g$ of the neat PMMA is 79.6 °C, where the value increased to 84.7 °C with inclusion of 0.5 wt % CNF-COOH, and further increased to 86.7 °C for a 3 wt % CNF-COOH/PMMA film. Only minor changes in $T_g$ are evident as the nanofibril content was increased above 3 wt %, with an apparent plateau at about 87 °C. A similar trend was observed on tan $\delta$ from dynamic mechanical analysis as discussed in the next section.

**Table 1. $T_g$ Data Table from DSC for the Neat PMMA Film and the PMMA/CNF-COOH Films**

| sample | DSC $T_g$ of PMMA (°C) |
|---|---|
| PMMA | 79.6 |
| PMMA/0.5% CNF-COOH | 84.7 |
| PMMA/1.0% CNF-COOH | 84.0 |
| PMMA/3.0% CNF-COOH | 86.7 |
| PMMA/5.0% CNF-COOH | 87.3 |

The influence of CNF-COOH on the thermal transition of PMMA could be explained by interactions between the acid groups on the nanofibrils and the ester groups of PMMA. This carbonyl oxygen in PMMA can physically interact with the carboxylic acid on the nanofibrils through hydrogen bonding (Scheme 1a). Generally speaking, the presence of hydrogen bonds should raise the value of $T_g$ because it restricts the motion of the polymer segments. This is consistent with the DSC results on the PMMA/CNF-COOH films. Hydrogen-bonding interactions between carboxylic acid groups and carbonyl groups have been widely used to facilitate miscibility of polymer blends[27] and to improve interfacial interactions of carbon nanotubes with PMMA.[28] In these cases, as is observed here, the hydrogen bonding was found to have a significant effect on the thermal properties of polymer nanocomposites. In addition, double hydrogen bonds are expected to form between groups of carboxylic acid on nanofibrils when the nanofibrils percolate within PMMA matrix, shown in Scheme 1b.

**Scheme 1. Schematic Illustrations of (a) Interfacial Interaction of Matrix PMMA with CNF-COOH and (b) Interaction between Percolated Nanofibrils**

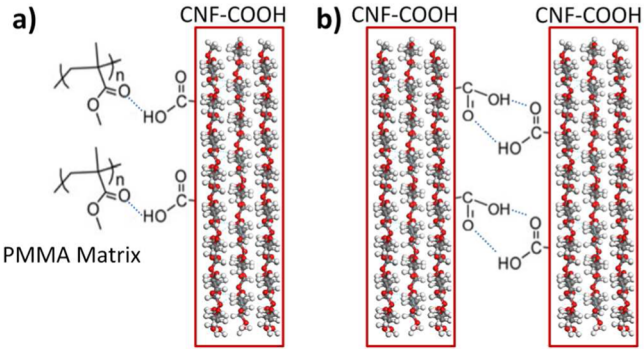


PMMA samples cast using different solvents have been extensively studied in the literature[29,30] to elucidate how the solvent affects the glass transition temperature of the polymer. Solvent-cast composite films obtained by the solution evaporation technique retain ∼5% solvent after evaporation and drying.[29] The retained solvent was found to significantly decrease the $T_g$ of the polymer in both experimental results[29] and modeling simulations.[30] For example, Mishra and Keten investigated the effect of retained solvent on the $T_g$ of PMMA through all-atom molecular dynamics simulations, and concluded that the addition of a weakly interactive solvent such as tetrahydrofuran (THF) caused a depression of the PMMA $T_g$.[30] Similar phenomenon was observed in this study. The retained solvent from the film preparation process decreased the $T_g$ values of both the neat PMMA film and the PMMA composite films. Continuous drying under high vacuum and 50 °C for several days did not effectively remove the retained solvent due to limited mobility of the PMMA chains at temperatures under $T_g$. Increasing the drying temperature to be above the $T_g$ of PMMA degrades the cellulose nanofibrils because of their limited thermal stability. Because the neat PMMA film and the PMMA/CNF-COOH films in this study were prepared under the same condition and CNF loading was kept to 5 wt % or below, differences in solvent retention due to CNFs were assumed to be negligible, and changes in $T_g$ and other properties observed between these two systems were only due to the addition of cellulose nanofibrils.

**Mechanical Properties and Fracture Surfaces.** In an attempt to examine the reinforcing effects of cellulose nanofibrils, we investigated dynamic mechanical and tensile properties of the nanocomposites. The neat PMMA has storage modulus of 2.1 GPa at 25 °C, where no apparent trend in the storage modulus was observed with increasing content of nanofibrils up to 5 wt %. With inclusion of 1 and 3 wt % CNF-COOH, the storage modulus values are to 1.5 and 2.0 GPa, respectively. The storage modulus increased to 3.5 GPa when the nanofibril content was increased to 5 wt %. Loss tangents (tan $\delta$) of CNF-COOH/PMMA as a function of temperature are shown in Figure 4. Neat PMMA shows a tan $\delta$ peak at 92.1 °C, which is attributed to its glass transition. The peak shifts to higher temperature for all of the PMMA/CNF-COOH nanocomposites. For example, PMMA/CNF-COOH at 1 wt % has a tan $\delta$ peak at 114.6 °C, which is 22.5 °C higher than the

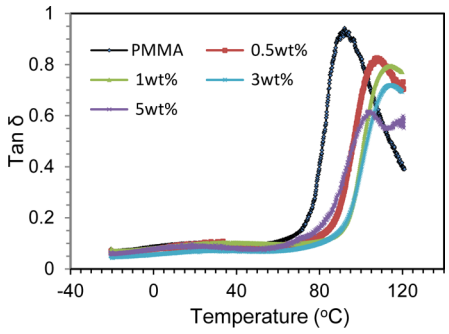


**Figure 4.** Tan $\delta$ of the PMMA films with and without the nanofibrils.


DOI: 10.1021/acsami.5b08317
ACS Appl. Mater. Interfaces 2015, 7, 25464−25472

neat PMMA. This is consistent with shifts in the glass transition observed in the DSC diagrams. As the movement of polymer chains is restricted because of confinement on the nanofibrils, increased energy is required for the polymer chains to become free to move. The magnitude of the tan $\delta$ peak for the nanocomposites decreased compared to the neat PMMA film. Increasing the nanofibril content diminishes the value of tan $\delta$, because the nanofibrils impose restrictions against molecular motion of surface adsorbed polymer chains, resulting in a more elastic response in the material.

The tensile behaviors of PMMA/CNF-COOH films were investigated by universal tensile tests. Representative strain−stress curves for the neat PMMA film and the PMMA/CNF-COOH films at various percentages of CNF-COOH are shown in Figure 5, and the tensile mechanical average values are

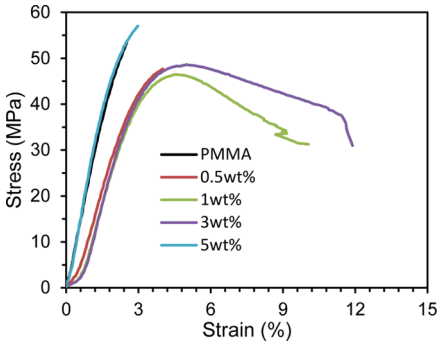


**Figure 5.** Representative stress−strain curves for the neat PMMA and the PMMA/CNF-COOH films.

**Table 2. Tensile Properties of PMMA/CNF-COOH Nanocomposite Films**

| CNF-COOH content (wt %) | Young's modulus (GPa) | ultimate strength (MPa) | strain-at-failure (%) | tensile toughness ($\times 10^3$ kJ/m$^3$) |
|---|---|---|---|---|
| 0 | 1.93 ± 0.15 | 53.2 ± 5.6 | 2.7 ± 0.3 | 0.84 ± 0.20 |
| 0.5 | 1.75 ± 0.08 | 45.4 ± 3.8 | 3.9 ± 0.6 | 1.14 ± 0.45 |
| 1 | 1.88 ± 0.10 | 45.9 ± 2.4 | 8.6 ± 3.3 | 2.74 ± 1.19 |
| 3 | 1.98 ± 0.03 | 47.2 ± 1.6 | 11.7 ± 0.4 | 4.08 ± 0.30 |
| 5 | 2.08 ± 0.10 | 56.6 ± 2.91 | 2.8 ± 0.2 | 0.94 ± 0.13 |

summarized in Table 2. The glassy PMMA film shows a typical brittle fracture with a strain-at-failure of 2.7%, which is consistent with previous report.[31] Addition of a small percentage of nanofibrils such as 0.5 wt % increases the strain-at-break value to 3.9%, though the tensile strength and Young's modulus decrease from 53.2 MPa and 1.93 GPa for neat PMMA to 45.4 MPa and 1.75 GPa, respectively. The increases in strain-at-failure are much more significant with nanofibrils 1 wt % of nanofibrils, reaching 8.6%. The strain-at-failure increases to 11.7% at 3 wt % CNF. Because of the significant increase in the strain-at-failure, the tensile toughness or deformation energy (the integrated area below the stress−strain curves) of the PMMA/CNF-COOH nanocomposites comprising 1 or 3 wt % cellulose nanofibrils are 3 times and 5 times greater, respectively, than the neat PMMA film. Further increasing the concentration of CNF-COOH to about 5 wt % resulted in brittle behavior with a strain-at-failure similar to that of the neat PMMA.

To probe the mechanism behind the toughness improvement, we have carried out scanning electron microscopy (SEM) studies to examine the fracture surfaces of the samples after the tensile tests. Figure 6 shows SEM images of fracture surfaces of

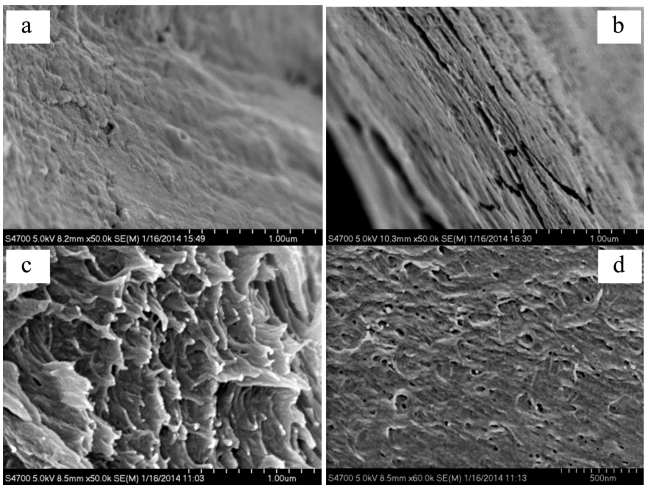


**Figure 6.** SEM images of tensile test samples: (a, b) fracture surfaces of the neat PMMA film, (c) fracture surface of PMMA/CNF-COOH (3 wt %), and (d) film surface near fracture of PMMA/CNF-COOH (3 wt %).

the PMMA film and the PMMA/CNF-COOH (3 wt %) film. As shown in Figure 6a, b, the PMMA film provides a smooth failure surface morphology, except for some residual fragments. The fracture surface of the nanocomposite (Figure 6c) is rougher than the neat PMMA, indicating the creation of additional surface area. The fracture surface of PMMA/CNF-COOH (3 wt %) also shows signs of plastic deformation, such as rough and irregular surface, which are in agreement with ductile fracture as demonstrated by its stress−strain curve. What appear to be nanofibrils are seen extending from the fracture surface, which suggest that the tensile strain failure occurred following break or pull-out of the nanofibrils. On the film surface next to the fracture (Figure 6d), holes and potential pull-out of nanofibrils are observed.

**Reinforcement Effect of the Nanofibrils.** At low nanofibril loading, the amount is generally too low to permit large-scale changes in material properties.[31] A concentration of nanofibrils below the percolation threshold will also allow unimpeded crack propagation across regions, which is similar to what is observed in the neat PMMA. When the content of nanofibrils was increased to 5%, some agglomerates form as described above. The inclusion of voids inside agglomerates can act as preferential sites for crack initiation, which leads to brittle failure and degrades the polymer performance.

With the addition of optimum amounts of cellulose nanofibrils, sufficient for the formation of a percolated network without much agglomeration in the composite, the PMMA composite undergoes a transition from brittle-to-ductile behavior with appearance of a yield point, and a tremendous increase in strain-to-failure (Figure 6). Reinforcement particles with longer length and higher aspect ratio reach percolation at lower filler contents. The critical percolation threshold (volume fraction) is a function of aspect ratio $L/w$; $\varphi_c = 0.7/(L/w)$, where $L$ and $w$ are the length and width of fibers, respectively.[5,32] The percolation threshold values of the nanofibrils in this study were calculated to be 0.64 vol % and


DOI: 10.1021/acsami.5b08317
ACS Appl. Mater. Interfaces 2015, 7, 25464−25472

0.87 wt %, using a PMMA density of 1.17 g/cm$^3$ and CNF density of 1.59 g/cm$^3$ in the calculation. When the content of nanofibrils in the composites reaches the percolation threshold, hydrogen bonding interactions are expected to form between carboxylic acid groups in the percolated nanofibrils (Scheme 1b). These nanofibril−nanofibril interactions contribute to further improvement in the mechanical properties of the composites by consuming additional energy that would otherwise cause it to break under the load.

An optimized nanofiber−matrix interface would allow for a combination of adequate stress transfer at low stress and frictional energy dissipation at higher stress.[11] For cellulose nanofibril reinforced hydrophobic polymer composites, it is widely observed that although one can improve the Young's modulus and even the stress at break by the addition of nanofibrils, the strain-to-failure and thus the toughness of the material are deleteriously affected. Improved tensile strength and Young's modulus were observed for composite films of CONF-COOH in polystyrene (PS);[9] however, these improvements are coupled with reduced elongation at break. Considering the molecular structure of polystyrene and the decrease in $T_g$ of the PS composites containing nanofibrils, the interfacial interactions between PS and CNF-COOH are considered to be weak. The very weak or no bonding between the matrix and nanofibrils leads to separation between the surfaces of nanofibrils and polymer under load. The crack initiates and propagates away from the interface into the polymer, resulting in premature failure of the polymer matrix at low strains. Thus, although nanofibrils are able to impart stiffness to the composite structure, they are not able to impart the expected toughness to the polymer matrix. In this study, the physical interactions via hydrogen bonding of nanofibrils with the polymer matrix and between percolated nanofibrils provide effective energy dissipation under the load, which prevent premature failure leading to strain and thus toughness improvement. However, toughening of PMMA in this study behaves like the ductile-brittle transition accompanied by decreased tensile strength. This is probably due to the use of interfacial hydrogen bonding interactions, which are relatively weak compared with covalent bonding and strong physical interactions. We expect that the toughness of the nanocomposites could be further improved without decreasing ultimate strength and modulus, by utilizing much stronger interactions than hydrogen bonds.

The results here demonstrate the potential of using cellulose nanofibrils to achieve enhanced toughness in hydrophobic glassy polymer composites. The importance of the interfacial region underscores the need for more detailed modeling and characterization to understand the polymer dynamics near nanofibrils.

**Simulation Results.** In the computational study, the neat polymer system is compared with the corresponding composite with a nanorod content of ∼1%. Figure 7a shows a representative image of the simulated composite system after equilibration. The structure is qualitatively similar to the TEM of the experimental films in Figure 3, illustrating well-dispersed nanorods at the onset of percolation.

To elucidate the role of favorable interfacial interaction between the polymer and the nanorods on properties, we varied the interfacial strength in the composite system. In composite system one (CR1), the polymer is attached to the nanorods via relatively strong bonding but weaker than covalent bonding. In the second system (CR2), there are no bonds between the polymer and the nanorods, only attractive Lennard−Jones interactions are present. These systems mimic composites with a strong-attractive or weak interface between the polymer and nanorods, respectively. Although both composite systems exhibit percolation of the nanorods, the polymer chains in CR1 are able to connect adjacent nanorods effectively forming "bridges" (Figure 7b).

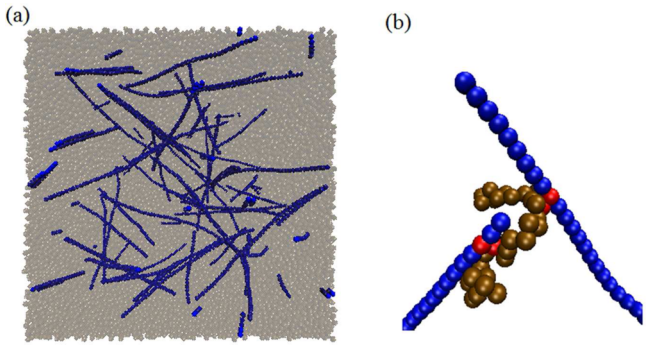


**Figure 7.** (a) Representative image of the polymer-nanorod composite obtained using coarse-grained simulation. Nanorods are shown in blue, polymer matrix is shown with transparent beads to improve clarity. (b) The polymer chain (shown in brown) can connect two nanorods through bonds. The connected particles are colored in red.

The equilibrated model systems were subjected to tensile deformation, where the stress−strain curve is shown in Figure 8a. The glassy, neat polymer system exhibits molecular-scale fracture by chain pullout during tensile deformation as a result of crazing. Instead of observing "sharp" fracture as in experiment where the impact of dangling ends on stress is

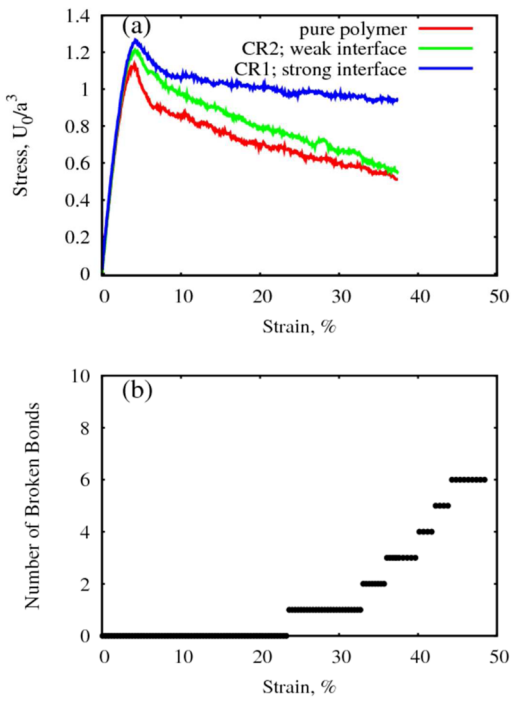


**Figure 8.** (a) True stress vs engineering strain curves obtained under uniaxial tension for the pure polymer and for the composite where the polymer and nanorod were allowed (CR1; relatively strong interface) or restricted (CR2; weak interface) during the equilibration process. (b) Number of broken polymer−nanorod bonds as a function of tensile deformation for CR1.


DOI: 10.1021/acsami.5b08317
ACS Appl. Mater. Interfaces 2015, 7, 25464−25472

inconsequential, the computed stress−strain curves exhibit a long "tail" after the maximal stress. This is a result of delayed pull-out of chains in the model and is, at least in part, due to the higher strain rate used in the simulations. In addition, due to the small system size of particle-based simulations, the simulated materials tend to fail in a more ductile fashion than experimental systems. In CR2, where the polymer matrix is not bonded to nanorods, the demonstrated deformation behavior is similar to the neat polymer. However, this composite system demonstrates a slight increase in the tensile modulus and the stress at break, which could be due to the impact of percolation of the nanoinclusions. This behavior is similar to the experimental system of polystyrene nanocomposites where the addition of CNF-COOH at a low concentration (less than 5% of nanorods) to a PS film only improved the tensile strength and Young's modulus.[9] On the other hand, CR1 that contains polymer−nanorod bonds, not only shows an increase in the tensile strength, but it also demonstrates more ductile behavior (Figure 8a). This behavior is similar to what was observed in the 1 wt % CNF-COOH PMMA composite described in previous section.

Our simulations results suggested that not only nanorod percolation, but also favorable polymer−rod interactions are important for improvement of toughness in these composites. Here, polymer "bridges" connect the nanorods, which provide additional toughening improvement through the formation of a polymer-nanorod network. Under deformation, these bridges can break at the polymer-nanorod interface (Figure 8b) providing an additional mechanism for energy dissipation. The CR2 system, which is unable to form these "bridges", shows only slight improvement in the mechanical properties.

There are deviations between the computed and experimental stress−strain curves due to restrictions in the computational model. The fracture that is observed experimentally occurs on the macroscale because of imperfections in the polymer sample such as cracks, notches, and extrinsic homogeneities. The size scale accessible to this simulation method is unable to capture these large-scale features and is instead restricted to molecular scale fracture, which is due to chain disentanglement or pullout and chain scission.[21] Even so, the goal of this work was not to accurately capture the fracture behavior of these materials, but to elucidate the fundamental mechanism responsible for toughening. In addition, coarse-grained models are physics-based models that lack chemical specificity. Nonetheless, they have been successfully used to study universal mechanisms and behavior exhibited by polymers.[33] Finally, as mentioned earlier, the strain rates required in this simulation method are higher than those used to obtain the experimental stress−strain curves.

Our approach focuses on overcoming traditional design limitations of polymer−nanorod composites by utilizing a combination of two major enhancement mechanisms: network creation and nanoparticle inclusions. The computational results suggest that percolation alone is insufficient for significant improvement of toughness. The favorable interfacial interactions together with percolation of nanofibril networks contribute to the toughness improvement observed in our systems.

## CONCLUSIONS

CNFs with surface carboxylic acid groups have been incorporated into PMMA matrix as reinforcement fillers. The resulting nanocomposite films have high transparency near that of the neat film due to very good dispersion of nanofibrils in PMMA. DSC analysis showed an increase in $T_g$ of the films prepared with CNF-COOH fillers in comparison with the neat PMMA film, providing evidence that interfacial interactions between PMMA and CNF-COOH are achieved. Mechanical analysis of the resulting films demonstrated that loadings of 1 and 3 wt % of CNF-COOH are effective reinforcing agents, and shift the failure mechanism to brittle-to-ductile failure behavior, yielding tougher films that those of neat PMMA. The fracture surface of the toughened films shows signs of plastic deformation, whereas PMMA film has brittle failure surface. The toughing effect of the nanofibrils has been probed by computational simulation. The simulation results suggest that favorable polymer−nanofibril interactions and the percolated nanofibril network contribute to the improvement of toughness in these composites.

Our study provides insights on CNF reinforcement of hydrophobic glassy polymers. The results suggest that judicious functionalization of nanofibril surfaces, which improve dispersion and enhance interfacial interactions, produces truly synergetic polymer composite materials. The success of improving toughness in a hydrophobic glassy polymer matrix indicates the possibility for prepare cellulosing nanofibril reinforced composites with controlled interface chemistry or interphase zones, and thus controlled mechanical properties.

## ASSOCIATED CONTENT

### Supporting Information

The Supporting Information is available free of charge on the ACS Publications website at DOI: 10.1021/acsami.5b08317.

STEM HAADF image of cross-sectional PMMA/CNF-COOH (3 wt %) film and DSC curves of PMMA and PMMA/CNF-COOH films (PDF)

## AUTHOR INFORMATION

### Corresponding Author

*E-mail: hong.dong.ctr@mail.mil. Phone: 301-3942415.

### Present Address

§H.D. is currently at U.S. Army Research Laboratory, Biotechnology Branch, Adelphi, MD 20783

### Notes

The authors declare no competing financial interest.

## ACKNOWLEDGMENTS

The research reported in this document was performed in connection with contract/instrument W911QX-14-C-0016 with the U.S. Army Research Laboratory. J. Steele was supported in part by an appointment to the Postgraduate Research Participation Program at the U.S. Army Research Laboratory administered by the Oak Ridge Institute for Science and Education through an interagency agreement between the U.S. Department of Energy and USARL. The authors thank Dr. Randy Mrozek, Dr. Erich Bain, and Mr. Eugene Napadensky at U.S. Army Research Laboratory for useful discussions.

## REFERENCES

(1) Postek, M. T.; Moon, R. J.; Rudie, A. W.; Bilodeau, M. A. *Production and Applications of Cellulose Nanomaterials*; TAPPI Press: Peachtree Corners, GA, 2013.

(2) Moon, R. J.; Martini, A.; Nairn, J.; Simonsen, J.; Youngblood, J. Cellulose Nanomaterials Review: Structure, Properties and Nanocomposites. *Chem. Soc. Rev.* **2011**, *40*, 3941−3994.



DOI: 10.1021/acsami.5b08317
*ACS Appl. Mater. Interfaces* 2015, 7, 25464−25472

(3) Isogai, A.; Saito, T.; Fukuzumi, H. TEMPO-Oxidized Cellulose Nanofibers. *Nanoscale* **2011**, *3*, 71−85.
(4) Kalia, S.; Boufi, S.; Celli, A.; Kango, S. Nanofibrillated Cellulose: Surface Modification and Potential Applications. *Colloid Polym. Sci.* **2014**, *292*, 5−31.
(5) Xu, X. Z.; Liu, F.; Jiang, L.; Zhu, J. Y.; Haagenson, D.; Wiesenborn, D. P. Cellulose Nanocrystals vs. Cellulose Nanofibrils: A Comparative Study on Their Microstructures and Effects as Polymer Reinforcing Agents. *ACS Appl. Mater. Interfaces* **2013**, *5*, 2999−3009.
(6) Liu, D. G.; Sun, X.; Tian, H. F.; Maiti, S.; Ma, Z. S. Effects of Cellulose Nanofibrils on the Structure and Properties on PVA Nanocomposites. *Cellulose* **2013**, *20*, 2981−2989.
(7) Abdul Khalil, H. P. S.; Davoudpour, Y.; Islam, M. N.; Mustapha, A.; Sudesh, K.; Dungani, R.; Jawaid, M. Production and Modification of Nanofibrillated Cellulose Using Various Mechanical Processes: A review. *Carbohydr. Polym.* **2014**, *99*, 649−665.
(8) Siqueira, G.; Bras, J.; Dufresne, A. Cellulose Whiskers versus Microfibrils: Influence of the Nature of the Nanoparticle and its Surface Functionalization on the Thermal and Mechanical Properties of Nanocomposites. *Biomacromolecules* **2009**, *10*, 425−432.
(9) Fujisawa, S.; Ikeuchi, T.; Takeuchi, M.; Saito, T.; Isogai, A. Superior Reinforcement Effect of TEMPO-Oxidized Cellulose Nanofibrils in Polystyrene Matrix: Optical, Thermal, and Mechanical Studies. *Biomacromolecules* **2012**, *13*, 2188−2194.
(10) Fujisawa, S.; Saito, T.; Kimura, S.; Iwata, T.; Isogai, A. Comparison of Mechanical Reinforcement Effects of Surface-Modified Cellulose Nanofibrils and Carbon Nanotubes in PLLA Composites. *Compos. Sci. Technol.* **2014**, *90*, 96−101.
(11) Moniruzzaman, M.; Winey, K. I. Polymer Nanocomposites Containing Carbon Nanotubes. *Macromolecules* **2006**, *39*, 5194−5205.
(12) Littunen, K.; Hippi, U.; Saarinen, T.; Seppala, J. Network Formation of Nanofibrillated Cellulose in Solution Blended Poly(methyl methacrylate) Composites. *Carbohydr. Polym.* **2013**, *91*, 183−190.
(13) Reiner, R. S.; Rudie, A. W. Pilot Plant Scale-up of TEMPO-Pretreated Cellulose Nanofibrils. In *Production and Applications of Cellulose Nanomaterials*; Postek, M. T.; Moon, R. J.; Rudie, A. W.; Bilodeau, M. A., Eds.; TAPPI Press: Peachtree Corners, GA, 2013; Chapter 2, pp 177−178.
(14) Okita, Y.; Fujisawa, S.; Saito, T.; Isogai, A. TEMPO-Oxidized Cellulose Nanofibrils Dispersed in Organic Solvents. *Biomacromolecules* **2011**, *12*, 518−522.
(15) http://lammps.sandia.gov, accessed from Oct 2014 to March 2015.
(16) Plimpton, S. Fast Parallel Algorithms for Short-Range Molecular-Dynamics. *J. Comput. Phys.* **1995**, *117*, 1−19.
(17) Kremer, K.; Grest, G. S. Molecular-Dynamics (MD) Simulations for Polymers. *J. Phys.: Condens. Matter* **1990**, *2*, Sa295−Sa298.
(18) Rottler, J. Fracture in Glassy Polymers: A Molecular Modeling Perspective. *J. Phys.: Condens. Matter* **2009**, *21*, 463101.
(19) Rottler, J.; Barsky, S.; Robbins, M. O. Cracks and Crazes: On Calculating the Macroscopic Fracture Energy of Glassy Polymers from Molecular Simulations. *Phys. Rev. Lett.* **2002**, *89*, 148304.
(20) Svaneborg, C.; Everaers, R.; Grest, G. S.; Curro, J. G. Connectivity and Entanglement Stress Contributions in Strained Polymer Networks. *Macromolecules* **2008**, *41*, 4920−4928.
(21) Sliozberg, Y. R.; Hoy, R. S.; Mrozek, R. A.; Lenhart, J. L.; Andzelm, J. W. Role of Entanglements and Bond Scission in High Strain-Rate Deformation of Polymer Gels. *Polymer* **2014**, *55*, 2543−2551.
(22) Sliozberg, Y. R.; Andzelm, J. W. Fast Protocol for Equilibration of Entangled and Branched Polymer Chains. *Chem. Phys. Lett.* **2012**, *523*, 139−143.
(23) Bennemann, C.; Paul, W.; Binder, K.; Dunweg, B. Molecular-Dynamics Simulations of the Thermal Glass Transition in Polymer Melts: Alpha-Relaxation Behavior. *Phys. Rev. E: Stat. Phys., Plasmas, Fluids, Relat. Interdiscip. Top.* **1998**, *57*, 843−851.
(24) Li, Q. Q.; Renneckar, S. Supramolecular Structure Characterization of Molecularly Thin Cellulose I Nanoparticles. *Biomacromolecules* **2011**, *12*, 650−659.
(25) Dong, H.; Snyder, J. F.; Tran, D. T.; Leadore, J. L. Hydrogel, Aerogel and Film of Cellulose Nanofibrils Functionalized with Silver Nanoparticles. *Carbohydr. Polym.* **2013**, *95*, 760−767.
(26) Dong, H.; Fey, E.; Gandelman, A.; Jones, W. E. Synthesis and Assembly of Metal Nanoparticles on Electrospun Poly(4-vinylpyridine) Fibers and Poly(4-vinylpyridine) Composite Fibers. *Chem. Mater.* **2006**, *18*, 2008−2011.
(27) Su, F. K.; Liau, G. F.; Hong, J. L. Restraining the Aggregation of Photoluminescent 1-Pyrenecarboxylic Acid by Hydrogen Bonding to Poly(methyl methacrylate). *J. Polym. Sci., Part B: Polym. Phys.* **2007**, *45*, 920−929.
(28) Madhukar, K.; Sainath, A. V. S.; Rao, B. S.; Kumar, D. S.; Bikshamaiah, N.; Srinivas, Y.; Babu, N. M.; Ashok, B. Role of Carboxylic Acid Functionalized Single Walled Carbon Nanotubes in Polyamide 6/Poly(methyl methacrylate) Blend. *Polym. Eng. Sci.* **2013**, *53*, 397−402.
(29) Patra, N.; Salerno, M.; Diaspro, A.; Athanassiou, A. Effect of Solvents on the Dynamic Viscoelastic Behavior of Poly(methyl methacrylate) Film Prepared by Solvent Casting. *J. Mater. Sci.* **2011**, *46*, 5044−5049.
(30) Mishra, S.; Keten, S. Atomistic Simulation Based Prediction of the Solvent Effect on the Molecular Mobility and Glass Transition of Poly(methyl methacrylate). *Appl. Phys. Lett.* **2013**, *102*, 041903.
(31) Ash, B. J.; Siegel, R. W.; Schadler, L. S. Mechanical Behavior of Alumina/Poly(methyl methacrylate) Nanocomposites. *Macromolecules* **2004**, *37*, 1358−1369.
(32) Favier, V.; Canova, G. R.; Shrivastava, S. C.; Cavaille, J. Y. Mechanical Percolation in Cellulose Whisker Nanocomposites. *Polym. Eng. Sci.* **1997**, *37*, 1732−1739.
(33) Baschnagel, J.; Wittmer, J. P.; Meyer, H. Monte Carlo Simulation of Polymers: Coarse-Grained Models. *arXiv preprint cond-mat* **2004**, 0407717.


DOI: 10.1021/acsami.5b08317
*ACS Appl. Mater. Interfaces* 2015, 7, 25464−25472